Control of the Casimir force by the modification of dielectric properties with light

F. Chen,[1] G. L. Klimchitskaya,[2] V. M. Mostepanenko,[3] and U. Mohideen[1]
[1]*Department of Physics and Astronomy, University of California, Riverside, California 92521, USA*
[2]*North-West Technical University, Millionnaya Strasse 5, St. Petersburg 191065, Russia*
[3]*Noncommercial Partnership "Scientific Instruments," Tverskaya Strasse 11, Moscow 103905, Russia*
(Received 11 April 2007; published 27 July 2007)

The experimental demonstration of the modification of the Casimir force [Proc. K. Ned. Akad. Wet. **51**, 793 (1948)] between a gold coated sphere and a single-crystal Si membrane by light pulses is performed. The specially designed and fabricated Si membrane was irradiated with 514 nm laser pulses of 5 ms width in high vacuum, leading to a change of the charge-carrier density. The difference in the Casimir force in the presence and in the absence of laser radiation was measured by means of an atomic force microscope as a function of separation at different powers of the absorbed light. The total experimental error of the measured force differences at a separation of 100 nm varies from 10% to 20% in different measurements. The experimental results are compared with theoretical computations using the Lifshitz theory [Zh. Eksp. Teor. Fiz. **29**, 94 (1956) [Sov. Phys. JETP **2**, 73 (1956)]; *Statistical Physics* (Pergamon, Oxford, 1981), Pt. II] at both zero and laboratory temperatures. The total theoretical error determined mostly by the uncertainty in the concentration of charge carriers when the light is incident is found to be about 14% at separations less than 140 nm. The experimental data are consistent with the Lifshitz theory at laboratory temperature, if the static dielectric permittivity of high-resistivity Si in the absence of light is assumed to be finite. If the dc conductivity of high-resistivity Si in the absence of light is included into the model of dielectric response, the Lifshitz theory at nonzero temperature is shown to be experimentally inconsistent at 95% confidence. The demonstrated phenomenon of the modification of the Casimir force through a change of the charge-carrier density is topical for applications of the Lifshitz theory to real materials in fields ranging from nanotechnology and condensed matter physics to the theory of fundamental interactions.

DOI: 10.1103/PhysRevB.76.035338 PACS number(s): 72.20.Jv, 78.20.Ci, 72.80.Ey, 85.85.+j

I. INTRODUCTION

After many years of pure academic research, the Casimir effect[1] is presently of much interest in connection with applications in nanomechanical devices,[2–4] noncontact friction,[5–8] carbon nanotubes,[9–12] Bose-Einstein condensation,[13,14] and for constraining predictions of modern unification theories of fundamental interactions.[15–19] These areas of application were made possible by extensive experimental investigation of the Casimir force[17–26] and the generalization to real materials of field-theoretical methods which were applicable to only idealized boundaries (see reviews[27,28]).

The basic theory of the Casimir and van der Waals forces at nonzero temperature proposed by Lifshitz[29,30] allows one to calculate all quantities of physical interest using the dielectric permittivity of boundary materials along the imaginary frequency axis. This theory was originally developed for the configuration of two semispaces and was later extended for any layer structure.[31–33] Using the proximity force theorem,[34] Lifshitz-type formulas for the configuration of a sphere or a cylinder above a plate were obtained and successfully used for the interpretation of experimental data.[3,17–24,26] For a long time, the lack of exact results for these configurations made it possible to question the validity of the comparison of experiment and theory based on the proximity force theorem. Recently, however, both the exact analytical[35–37] and numerical[38] results for the Casimir force between a sphere (cylinder) and a plate were obtained, demonstrating that at small z the corrections to the proximity force theorem for both configurations are, in fact, less than z/R (z is the separation between a cylinder or a sphere of radius R and a plate), i.e., less than it was supposed in the comparison of experiment with theory. Thus, the use of the proximity force theorem in Refs. 3, 17–24, and 26 and below is substantiated on the basis of first principles of quantum field theory.

The vital issue in many applications of the Casimir effect is how to control the magnitude of the force by changing the parameters of the system. In this respect, the possibility that the Casimir force can change sign from attraction to repulsion depending on system geometry is of much importance. It may be used to prevent collapse of small mechanical elements onto nearby surfaces in nanodevices.[39] However, the Casimir repulsion has yet to be observed experimentally. An alternative method to control the magnitude of the Casimir force is to change the material properties of the interacting bodies. In Ref. 40, the Casimir force was measured acting between a plate and a sphere coated with a hydrogen-switchable mirror that becomes transparent upon hydrogenation. Despite expectations, no significant decrease of the Casimir force owing to the increased transparency of the plates was observed. The negative result is explained by the Lifshitz theory which requires the change of the reflectivity properties within a wide range of frequencies in order to markedly affect the magnitude of the Casimir force. This requirement is not satisfied by the hydrogenation.

All modern experiments on the measurement of the Casimir force mentioned above[3,17–26,40] used metallic test bodies. Metallic surfaces are necessary to reduce and compensate the effects of residual charges and work function differences. It is, however, hard to modify their reflectivity

properties over a sufficiently wide range of frequencies. The appropriate materials for the control, modification, and fine tuning of the Casimir force are semiconductors. The reflectivity properties of semiconductor surfaces can be changed in a wide frequency range by changing the carrier density through the variation of temperature, using different kinds of doping, or, alternatively, via the illumination of the surface with laser light. At the same time, semiconductor surfaces with reasonably high conductivity avoid accumulation of excess charges and, thus, preserve the advantage of metals. In addition, as semiconductors are the basic fabrication materials for nanotechnology, the use of semiconductor surfaces for the control of the Casimir force will lead to many applications.

The modification of the Casimir force between a gold coated plate and a sphere, attached to the cantilever of an atomic force microscope (AFM), through the variation of temperature was considered in Ref. 41. While changing the temperature to modify the carrier density in semiconductors is a good method in theory, it leads[42] to large systematic errors in the measurement setup using the AFM. In Ref. 43, the Casimir force between a gold coated sphere and a single-crystal B-doped Si plate was measured in high vacuum. It was found that the force between a metal and a semiconductor decreases with the increase of separation more quickly than between two metals. In Ref. 44, the experimental data for the Casimir force between a gold coated sphere and a B-doped Si plate were compared with two different theoretical computations, one made for the B-doped Si used and another one for high-resistivity Si. It was shown that the computation using the tabulated optical data for high-resistivity Si is excluded by experiment at 70% confidence, while the theoretical results computed for the plate used in experiment are consistent with data. In Ref. 45, the difference in the Casimir forces between a gold coated sphere and two P-doped Si plates with different charge-carrier densities was directly measured at a 95% confidence level. This demonstrates that the change of carrier density due to doping leads to noticeable modification of the Casimir force.

The most suitable method to change the carrier density in semiconductors is through the illumination of the surfaces by laser light (see, e.g., Refs. 46 and 47). An early attempt to measure the van der Waals and the Casimir forces between semiconductors and modify them with light was reported in Ref. 48. Attractive forces were measured between a glass lens and a Si plate and also between a glass lens coated with amorphous Si and a Si plate. However, the glass lens is an insulator and therefore the electric forces such as due to work function potential differences could not be controlled. This might also explain that no force change occurred on illumination at separations below 350 nm,[48] where it should have been most pronounced.

The present paper contains the detailed results of our experiments on the modification of the Casimir force by the irradiation of a Si membrane with laser pulses. An observation of this effect at only one absorbed power was briefly reported in Ref. 49. Here, we report measurements performed at different absorbed powers and the theoretical analysis on the accuracy of the obtained results and on the comparison of experiment with theory. In our experiments, the carrier density in the Si membrane is changed by the incident light, and the difference in the Casimir force acting between that membrane and the gold coated sphere in the presence and in the absence of light is measured. The experimental error of difference force measurements for the different absorbed powers determined at a 95% confidence level varies between 10% and 20% at a separation of 100 nm and increases with the increase of separation. The measurement data collected at different powers of the incident light at the laboratory temperature $T=300$ K were compared with the Lifshitz theory at both zero and laboratory temperatures. The data are shown to be consistent with theory at laboratory temperature if in the absence of light the static dielectric permittivity of Si is assumed to be finite. The Lifshitz theory at laboratory temperature taking account of the dc conductivity of high-resistivity Si in the absence of light is excluded experimentally at a 95% confidence level. Thus, our experiments not only demonstrate the modification of the Casimir force through the irradiation of a semiconductor surface but also lead to the important result that the inclusion of zero-frequency conductivity of high-resistivity Si in the model of dielectric response results in a contradiction between the Lifshitz theory at laboratory temperature and experiment. This contradiction is caused by different contributions from the reflection of the transverse magnetic mode on a Si surface at zero frequency in the absence and in the presence of conductivity. The obtained conclusion supports recent theoretical results that the inclusion of dielectric dc conductivity for the dielectric-dielectric[8] and dielectric-metal[50,51] configurations at nonzero temperature leads to contradiction between the Lifshitz theory and the Nernst heat theorem, and thus such inclusion is impermissible. At the same time, the experimental data are shown to be consistent with the Lifshitz theory at zero temperature, irrespective of whether the dc conductivity of high-resistivity Si is included or not.

The paper is organized as follows. In Sec. II, the experimental setup and sample preparation are described. Section III contains the description of the measurement procedure and obtained experimental results. This includes the calibration of the setup, the measurement of the lifetime of excited carriers, the measurement of the difference in the Casimir force when the light is on and off, and the analysis of the experimental errors. In Sec. IV, the experimental results are compared with the theory. Here, the difference in the Casimir force with and without incident laser light is calculated and the theoretical errors are analyzed. By combining the experimental and theoretical errors, the quantitative measure of agreement between experiment and theory at 95% confidence is presented. Section V analyzes the role of the dc conductivity of high-resistivity Si in the Casimir force. Section VI contains our conclusions and discussion.

II. EXPERIMENTAL SETUP AND SAMPLE PREPARATION

Here, we discuss the experimental setup used to demonstrate the modification of the Casimir force through the radiation induced change in the carrier density. The general scheme of the setup is shown in Fig. 1. A high vacuum based AFM was employed to measure the change in the Casimir

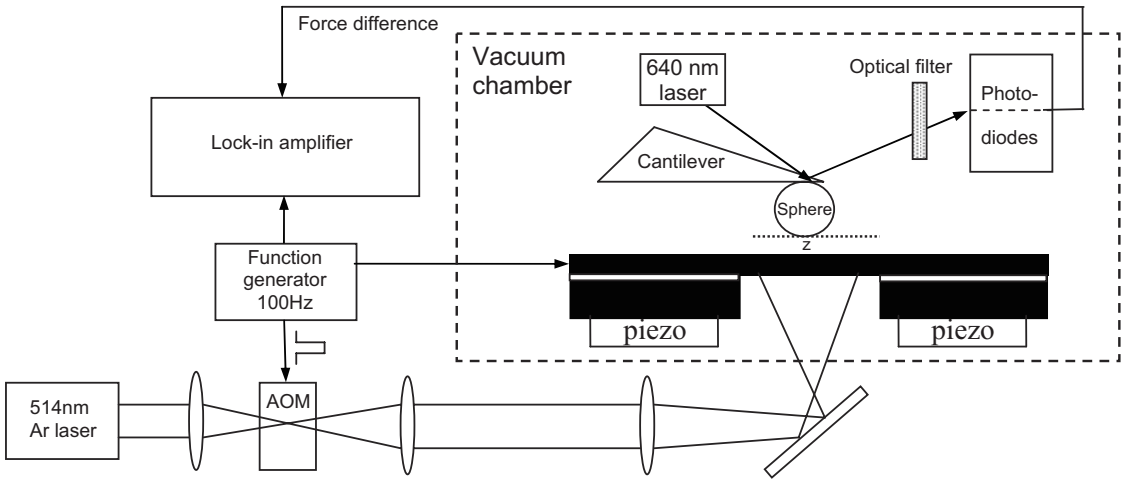

FIG. 1. Schematic of the experimental setup, showing its main components (see text).

force between a gold coated sphere of diameter $2R = 197.8 \pm 0.3$ μm and a Si membrane (colored black) in the presence and in the absence of incident light. An oil-free vacuum chamber with a pressure of around 2×10^{-7} Torr was used. The polystyrene sphere coated with a gold layer of 82 ± 2 nm thickness was mounted at the tip of a 320 μm conductive cantilever (see Fig. 1). The Si membrane (see below for the process of its preparation) was mounted on top of a piezo which is used to change the separation distance z between the sphere and the membrane from contact to 6 μm. The excitation of the carriers in the Si membrane was done with 5 ms wide light pulses (50% duty cycle). These pulses were obtained from a cw Ar ion laser light at 514 nm wavelength modulated at a frequency of 100 Hz using an acousto-optic modulator (AOM). The AOM is triggered with a function generator. The laser pulses were focused on the bottom surface of the Si membrane. The Gaussian width of the focused beam on the membrane was measured to be 0.23 ± 0.01 mm.

The cantilever of the AFM flexes when the Casimir force between the sphere and the membrane changes depending on the presence or the absence of incident light on the membrane. This cantilever deflection is monitored with a 640 nm beam from an additional laser (see Fig. 1) reflected off the top of the cantilever tip. An optical filter was used to prevent the interference of the 514 nm excitation light with the cantilever deflection signal. The transmission of this filter at 514 nm is 0.001%. Including the less than 1% transmission through the Si membrane and the diode solid angle of 10^{-4}, the impact of the 514 nm light leakage leads to less than 10^{-6} pN changes in the force difference. These changes are negligibly small as compared with the measured cantilever deflection signal. The latter leads to a difference signal between the two photodiodes. The resulting modification of the Casimir force in response to the carrier excitation is measured with a lock-in amplifier. The same function generator signal used to generate the Ar laser pulses is also used as a reference for the lock-in amplifier.

The most important part of the setup is the Si membrane. It should be sufficiently thin and of high resistivity to ensure that the density of charge carriers increases by several orders of magnitude under the influence of the laser pulses. The Si membrane should be thick enough to make negligible the photon pressure of the transmitted light, as the illumination is incident on the bottom surface of the membrane (see Sec. IV B for details). The thickness of the Si membrane has to be greater than 1 μm, i.e., greater than the optical absorption depth of Si at the wavelength of the laser pulses. Fabrication of the few micrometer thick Si membrane with the necessary properties is described below.

A commercial Si grown on an insulator wafer was used as the initial product. The insulator in this case is SiO_2, which is the native oxide of Si and thus leads to only small reductions of the excited carrier lifetime in Si. A layout of the wafer is shown in Fig. 2. The wafer consists of a Si substrate of 600 μm thickness and a Si top layer of 5 μm thickness (both are single crystals and have a $\langle 100 \rangle$ crystal orientation) with the buried intermediate SiO_2 layer of thickness 400 nm [see Fig. 2(a)]. The Si is p-type doped with relatively high nominal resistivity of about 10 Ω cm. The corresponding carrier density is equal to $\tilde{n} \approx 5 \times 10^{14}$ cm^{-3}.[52]

The thickness of the Si substrate is reduced to about 200 μm through mechanical polishing. Then, after RCA cleaning of the surface, the wafer is oxidized at $T = 1373$ K in a dry O_2 atmosphere for a duration of 72 h. As a result, in addition to the buried SiO_2 layer, a thermal oxide layer with

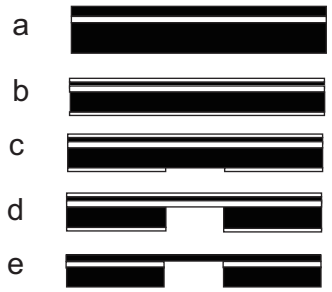

FIG. 2. Fabrication process of Si membrane. (a) The Si substrate (colored black) with a buried SiO_2 layer (white). (b) The substrate is mechanically polished and oxidized, and (c) a window in SiO_2 is etched with HF. (d) Next, TMAH is used to etch the Si. (e) Finally, SiO_2 layer is etched away in HF solution to form a clean Si surface.

a thickness of about 1 μm is formed on both (bottom and top) sides of the wafer [Fig. 2(b)]. This oxide layer serves as a mask for subsequent tetramethylammonium hydroxide (TMAH) etching of the Si. First, a hole with the diameter of 0.85 mm is etched with HF in the center of the bottom oxidation layer [Fig. 2(c)]. This exposes the Si substrate. Next, TMAH is used at 363 K to etch the Si substrate through the hole formed in the oxide mask [Fig. 2(d)]. Note that TMAH selectively etches Si as its etching rate for Si is 1000 times greater than for SiO_2. TMAH etching leads to the formation of a hole through the Si substrate. Given the selectivity of the etching, the buried 400 nm oxide is the stop etch layer. Finally, all the thermal oxidation layers and buried oxidation layer in the hole are etched away in HF solution to form a clean Si membrane over the hole as in Fig. 2(e). The thickness of this membrane was measured to be 4.0 ± 0.3 μm using an optical microscope. In order for voltages to be applied to the Si membrane, an ohmic contact is formed by a thin film of Au deposited on the edge of the membrane followed by annealing at 673 K for 10 min. The Si membrane was cleaned with Nanostrip and then passivated by dipping in 49% HF for 10 s. The passivated Si membrane was then mounted on top of the piezo as described above.

III. MEASURING PROCEDURE AND EXPERIMENTAL RESULTS

A. Calibration of the setup

All calibrations and other measurements are done at the same period of time as the measurement of the difference of Casimir forces and in the same high vacuum apparatus. The calibration of the deflection signal of the cantilever from the photodiodes, S_{def}, and the determination of the separation on contact and residual potential difference between the gold coated sphere and Si membrane are done by measuring the distance dependence of an applied electrostatic force. For this purpose, the same function generator (see Fig. 1) is used for applying voltages to the membrane. For an attractive force, $S_{\mathrm{def}}<0$ and can be measured either as a current or as a voltage. In addition, a small correction has to be applied to the separation distance between the gold sphere and the Si membrane due to the movement of the cantilever. The actual separation distance z between the bottom of the sphere and the membrane is given by

$$z = z_{\mathrm{piezo}} + mS_{\mathrm{def}} + z_0. \tag{1}$$

Here, z_{piezo} is the distance moved by the piezo, m is the deflection coefficient in units of nanometer per unit deflection signal, and z_0 is the average separation on contact of the gold surface and Si membrane. z_0 is nonzero due to the stochastic roughness of the surfaces. The complete movement of the piezo was calibrated using a fiber optic interferometer. To extend and contract the piezo, continuous triangular voltages between 0.01 and 0.02 Hz are applied to it. Given that the experiment is done at room temperature, applying static voltages would lead to piezo creep and loss of position sensitivity. The deflection coefficient m can also be measured by the application of electrostatic forces between the sphere and the membrane.

In our measurements, the gold sphere was kept grounded. The electric contact to the sphere was accomplished by applying a very thin gold coating to the cantilever. The electrostatic force between the sphere and the membrane is given by[53]

$$F_e(z) = 2\pi\varepsilon_0(V-V_0)^2\sum_{n=1}^{\infty}\frac{\coth\alpha - n\coth n\alpha}{\sinh n\alpha}, \tag{2}$$

where V is the voltage applied to the Si membrane, V_0 is the residual potential difference between the grounded sphere and membrane, $\cosh\alpha=1+z/R$, and ε_0 is the permittivity of vacuum. The nonzero value of z at contact, z_0, is due to the surface roughness. In the complete measurement range of the electrostatic force from contact to 6 μm, Eq. (2) can be rearranged to the following simpler form within the limits of relative error less than 10^{-4} (Ref. 44):

$$F(z) = -2\pi\varepsilon_0(V-V_0)^2\sum_{i=-1}^{6} c_i\left(\frac{z}{R}\right)^i \equiv X(z)(V-V_0)^2, \tag{3}$$

where

$$c_{-1}=0.5, \quad c_0=-1.182\,60, \quad c_1=22.2375,$$
$$c_2=-571.366,$$

$$c_3=9592.45, \quad c_4=-90\,200.5, \quad c_5=383\,084,$$
$$c_6=-300\,357.$$

First, 30 different dc voltages between 0.65 and −0.91 V are applied to the Si membrane. The cantilever deflection signal is measured as a function of the distance. The 0.02 Hz triangular wave was applied to the piezo to change the distance between the sphere and the membrane over a range of 6 μm. Larger applied voltages lead to more cantilever deflection and, according to Eq. (1), to a contact of the two surfaces at larger z_{piezo}. The dependence of z_{piezo} at contact of the sphere and the membrane on the applied voltage can then be used to measure the deflection coefficient m. In order to determine the contact of the two surfaces precisely, 32 768 data points at equal time intervals were acquired for each force measurement (i.e., the interval between two points was about 0.18 nm). In cases where the contact point was between two neighboring data points, a linear interpolation was used to identify the exact value. The deflection coefficient was found to be $m=137.2\pm0.6$ nm per unit deflection signal. The difference in the value of m from previous measurements[24,43,44] is due to the use of the 514 nm filter which reduced the cantilever deflection signal. The obtained value of m was used to correct the separation distance in all measurements in accordance with Eq. (1). The electrostatic force resulting from the application of the dc voltages is also used in the determination of the separation on contact of the two surfaces. The fit of the experimental force-distance relation to the theoretical Eq. (3) is done as outlined in our previous work.[24,43,44] The separation distance on contact was determined to be $z_0=97$ nm. The uncertainty in the quantity

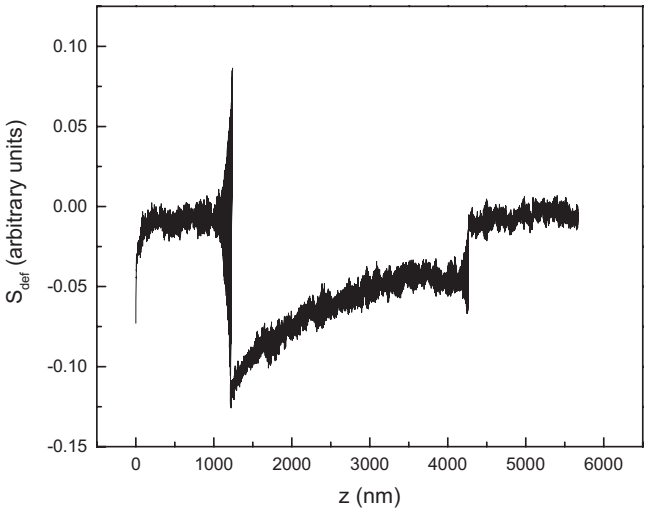

FIG. 3. The deflection signal of the cantilever in response to the dc voltage and square voltage pulse applied to the Si membrane as a function of separation.

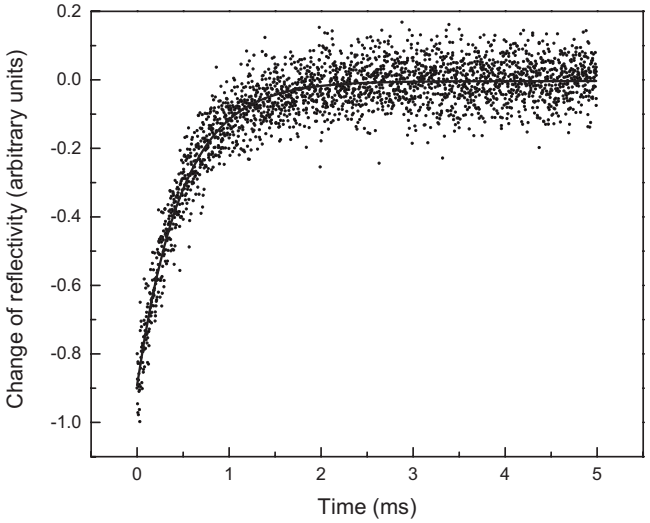

FIG. 4. The change of the reflectivity after the termination of the laser pulse.

z_0+mS_{def} from Eq. (1) was found to be 1 nm. This leads to the same error in absolute separations $\Delta z=1$ nm because the error in piezo calibration is negligibly small.

For the calibration of the deflection signal and the determination of the residual potential difference between the two surfaces, an improved method, rather than a simple application of the dc voltages to the membrane, was used. This was done to avoid systematic errors due to scattered laser light. In addition to the application of the dc voltage to the membrane, described above, square voltage pulse of amplitudes from 1.2 to −0.6 V and time interval corresponding to a separation distance between 1 and 5 μm was also applied to the membrane. Figure 3 shows the deflection signal of the cantilever in response to both the applied dc voltage and the square pulse as a function of the separation distance between the gold sphere and the Si membrane. By measuring only the difference in signal during the pulse allows one to avoid the need for a background subtraction. The fit of the difference signal to Eq. (3) leads to the value of the signal calibration constant 6.16 ± 0.04 nN per unit deflection signal. The same fit was used to determine the residual potential difference between the sphere and the membrane which was found to be $V_0=-0.171\pm0.002$ V. The large width of the pulse applied in addition to the dc voltage allowed confirmation of the distance independence of the obtained values of the calibration constant and the residual potential difference.

B. Excited carrier lifetime measurement

An independent measurement of the lifetime of the carriers excited in the Si membrane by the pulses from the Ar laser was performed. For this purpose, a noninvasive optical pump-probe technique was used.[54,55] The same Si membrane and Ar laser beam modulated by the AOM at 100 Hz to produce 5 ms wide square light pulses, as used in the Casimir force measurement, were employed as the sample and the pump, respectively. The diameter of the pump beam on the sample was measured to be 0.72 ± 0.02 mm. A cw beam with a 1 mW power at a wavelength of 1300 nm was used as a probe. The probe beam photon energy is below the band gap energy of Si and is thus not involved in carrier generation. This beam was focused to a Gaussian width size $w_0=0.135\pm0.003$ mm. Thus, the focal spot size of the probe beam is much smaller than the focal spot size of the pump light. This allowed one to measure the lifetime in a homogeneous region of excited carriers. The change in the reflected intensity of the probe beam in the presence and in the absence of Ar laser pulses was detected with an InGaAs photodiode. The change in reflected power of the probe beam was monitored as a function of time in an oscilloscope and found to be consistent with the change of carrier density. Near normal incidence for the pump and probe beams was used, with care taken to make sure that the InGaAs photodiode was isolated from the pump beam. The time decay of the reflected probe beam in response to the square Ar light pulses is shown in Fig. 4. The change of the reflectivity of the probe is fitted to an exponential of the form $-\exp(-t/\tau)$, where τ is the effective carrier lifetime. By fitting the whole 5 ms decay of the change in reflected power, the effective excited carrier lifetime was measured to be $\tau=0.47\pm0.01$ ms. Note that this time represents both surface and bulk recombination and is consistent with that expected for Si. Some dependence of the lifetime of the excited carriers on their concentration was observed. In the first 0.5 ms, while the concentration is still high enough, the average value of the excited carrier lifetime was measured to be $\tau=0.38\pm0.03$ ms. The measured values of the carrier lifetime will be used in Sec. IV A in the theoretical computations of the Casimir force differences for the comparison with several measurements having varying power of the Ar laser.

C. Experimental results and error analysis

Here, we present the determination of the difference in the Casimir force resulting from the irradiation of the Si membrane with 514 nm laser pulses. In fact, it is the difference in

the total force (Casimir and electric) which is measured. As was indicated above, even with no applied voltages there is some residual potential difference V_0 between the sphere and the membrane. The preliminary value of V_0 was determined during the calibration of the setup in the absence of laser pulses. In the presence of pulses (even during the dark phases of a pulse train), the values of the residual potential difference can be different. We represent these residual potential differences during the bright and dark phases of a laser pulse train (the latter is not exactly equal to the one determined in calibration) V_0^l and V_0, respectively. During the bright phases of the pulse train, we apply to the Si membrane the voltage V^l and during the dark phases the voltage V. Using Eq. (3) for the electric force, we can represent the difference in the total force (electric and Casimir) for the states with and without carrier excitation in the following form:

$$\Delta F_{\text{tot}}(z) = X(z)[(V^l - V_0^l)^2 - (V - V_0)^2] + \Delta F_C(z). \quad (4)$$

Here,

$$\Delta F_C(z) = F_C^l(z) - F_C(z) \quad (5)$$

is the difference in the Casimir force and F_C^l (F_C) is the Casimir force with (without) light. The difference in the total force in Eq. (4) was measured by the lock-in amplifier with an integration time constant of 100 ms, which corresponds to a bandwidth of 0.78 Hz. The measurement procedure is described below.

First, we kept V=const and changed V^l. The parabolic dependence of ΔF_{tot} on V^l in Eq. (4) was measured at different separations z. Care should be taken to apply only small voltage amplitudes (up to a few tens of millivolts) so as to keep the space charge region negligible. At every measured separation distance, ΔF_{tot} is plotted as a function of V^l. As is seen in Eq. (4), the value of V^l where the parabola reaches a maximum is V_0^l [recall that $X(z)<0$]. In this way, the value $V_0^l = -0.303 \pm 0.002$ V was found and shown to be independent of the separation from 100 to 500 nm where the difference in the Casimir force can be measured. Next, we kept V^l=const, changed V, and measured the parabolic dependence of ΔF_{tot} on V at different separations. The value of V where parabolas reach minima is $V_0 = -0.225 \pm 0.002$ V. These values of the residual potential difference between the sphere and the membrane in the presence and in the absence of excitation light were substituted in Eq. (4). The small change of around 78 mV in the residual potential difference between the sphere and the membrane in the presence and in the absence of excitation light is primarily due to the screening of surface states by few of the optically excited electrons and holes. The above small value is equal to the change in band bending at the surface. It is consistent with the fact that almost flat bands are obtained at the surface with the surface passivation technique used (see, e.g., Refs. 56 and 57).

Then, other voltages (V^l, V) were applied to the Si membrane and the difference in the total force ΔF_{tot} was measured as a function of separation. Data were collected from contact at equal time intervals corresponding to three points per 1 nm (i.e., in 1209 points within the separation interval from 100 to 500 nm). From these measurement results, the difference in the Casimir force $\Delta F_C^{\text{expt}}(z)$ was determined from Eq. (4). This procedure was repeated with some number of pairs (J) of different applied voltages (V^l, V) and at each separation the mean value $\langle \Delta F_C^{\text{expt}}(z) \rangle$ was found. In Fig. 5, the experimental data for $\langle \Delta F_C^{\text{expt}}(z) \rangle$ as a function of separation are shown by dots for different absorbed laser powers: P^{eff}=9.3 mW (J=31), 8.5 mW (J=41), and 4.7 mW

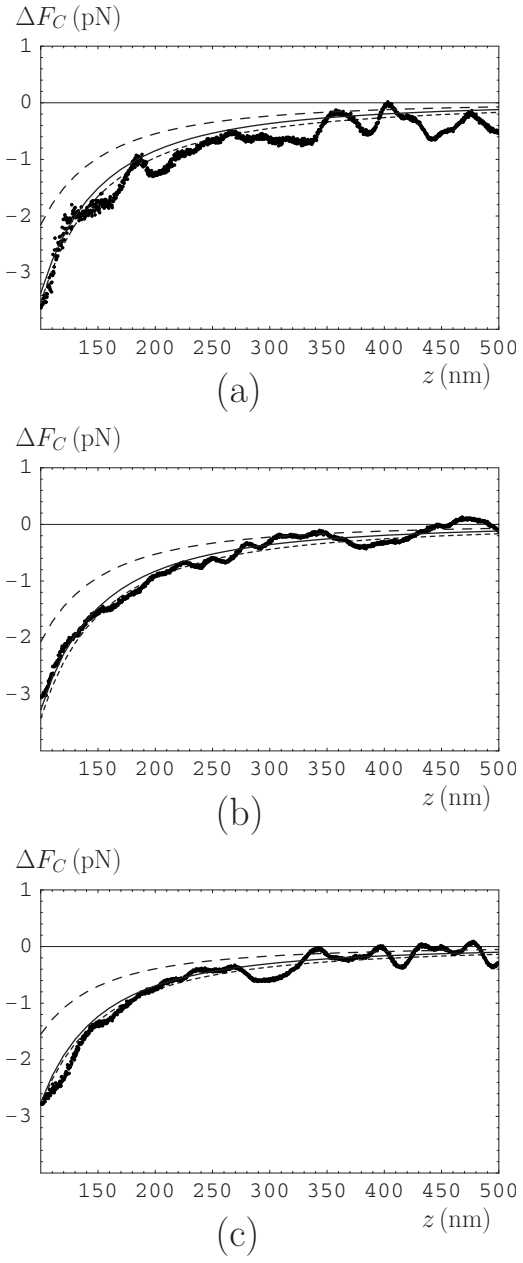

FIG. 5. The differences of the Casimir forces in the presence and in the absence of light versus separation for different absorbed powers: (a) 9.3 mW, (b) 8.5 mW, and (c) 4.7 mW. The measured differences $\langle \Delta F_C^{\text{expt}} \rangle$ are shown as dots, differences calculated using the Lifshitz formula at T=300 K, $\Delta F_C^{\text{theor}}$, and at T=0, $\Delta F_C^{\text{theor}}(T=0)$, as the solid and short-dashed lines, respectively, and those calculated including the dc conductivity of high-resistivity Si, $\Delta \tilde{F}_C^{\text{theor}}$, as the long-dashed lines.

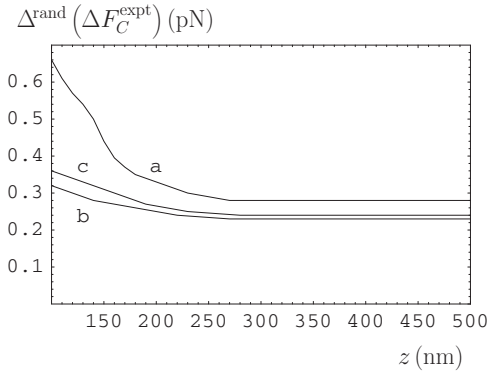

FIG. 6. The random errors (which are equal to the total) versus separation for the measurements with the different absorbed powers: *a*, 9.3 mW; *b*, 8.5 mW; and *c*, 4.7 mW.

($J=33$) in Figures 5(a)–5(c), respectively. The corresponding incident powers were 15.0, 13.7, and 7.6 mW, respectively. As expected, the magnitude of the Casimir force difference has the largest values at the shortest separations and decreases with the increase of separation. It also decreases with the decrease of the absorbed laser powers (the solid, short-, and long-dashed lines in Fig. 5 are explained in Sec. IV devoted to the comparison with theory).

Now, we proceed with the analysis of the experimental errors. The variance of the mean difference in the Casimir force is defined as

$$s_{\langle \Delta F_C^{\mathrm{expt}} \rangle}(z_i) = \left\{ \frac{1}{J(J-1)} \sum_{j=1}^{J} \left[\Delta F_C^{\mathrm{expt}}(z_{ij}) - \langle \Delta F_C^{\mathrm{expt}}(z_i) \rangle \right]^2 \right\}^{1/2}, \tag{6}$$

where i is the number of points in one set of measurements changing from 1 to 1209, and j is the number of the pair of the applied voltages. Using Student's t distribution with a number of degrees of freedom $f=30$ (or 40 and 32 for the measurements with different absorbed powers) and choosing $\beta=0.95$ confidence, we obtain $p=(1+\beta)/2=0.975$ and $t_p(f)=2.00$. Thus, the absolute random error in the measurement of the difference Casimir force is given by

$$\Delta^{\mathrm{rand}}(\Delta F_C^{\mathrm{expt}}(z)) = s_{\langle \Delta F_C^{\mathrm{expt}} \rangle}(z) t_p(f). \tag{7}$$

In this experiment, the random error is separation dependent. It is presented in Fig. 6 as a function of separation for the three different measurements with different absorbed laser powers (lines *a*, *b*, and *c* correspond to decreasing power indicated above). As is seen in Fig. 6, the random error is rather different for different measurements. It is the lowest for measurement *b* which was done with 8.5 mW absorbed power. In this measurement, the random error decreases from 0.32 pN at $z=100$ nm to 0.23 pN at $z=250$ nm and preserves the latter value at larger separations.

The main systematic error is due to the instrumental noise and is equal to $\Delta_1^{\mathrm{syst}}(\Delta F_C^{\mathrm{expt}}) \approx 0.08$ pN independent of separation. The systematic error determined from the resolution error in data acquisition, $\Delta_2^{\mathrm{syst}}(\Delta F_C^{\mathrm{expt}}) \approx 0.02$ pN, also does not depend on separation. The calibration error, $\Delta_3^{\mathrm{syst}}(\Delta F_C^{\mathrm{expt}})$, depends on separation and is equal to 0.6% of the measured difference in the Casimir force. These systematic errors are random quantities characterized by a uniform distribution. They can be combined at a given confidence probability β with the help of statistical criterion[58]

$$\Delta^{\mathrm{syst}}(\Delta F_C^{\mathrm{expt}}) = \min \left\{ \sum_{i=1}^{q} \Delta_i^{\mathrm{syst}}(\Delta F_C^{\mathrm{expt}}), k_\beta^{(q)} \sqrt{\sum_{i=1}^{q} [\Delta_i^{\mathrm{syst}}(\Delta F_C^{\mathrm{expt}})]^2} \right\}, \tag{8}$$

where $k_\beta^{(q)}$ is a tabulated coefficient. In our experiment, there are $q=3$ systematic errors listed above and at $\beta=0.95$ (95% confidence level) $k_{0.95}^{(3)}=1.12$. As a result, from Eq. (8) we arrive at the total systematic error for all three measurements varying from 0.092 to 0.095 pN.

The total experimental error of the force difference, $\Delta^{\mathrm{tot}}(\Delta F_C^{\mathrm{expt}}(z))$, at 95% confidence can be found by the combination of random and systematic errors. This is done using the statistical rule described in Ref. 58 and applied to the Casimir force measurements in Refs. 18, 44, and 59. According to this rule, the total error is equal to the random one if, as is the case in our experiments, the inequality

$$r(z) \equiv \frac{\Delta^{\mathrm{syst}}(\Delta F_C^{\mathrm{expt}}(z))}{s_{\langle F_C^{\mathrm{expt}} \rangle}(z)} \leqslant 0.8 \tag{9}$$

is satisfied. Thus, the total experimental error in the values of $\Delta F_C^{\mathrm{expt}}(z)$ for all three measurements as a function of the separation is presented in Fig. 6. As a result, the relative experimental error changes from 10% to 20% at a separation $z=100$ nm and from 25% to 33% at a separation $z=180$ nm for different absorbed laser powers. This allows us to conclude that the modulation of the dispersion force with light is demonstrated at a high reliability and confidence. The observed effect cannot be due to the mechanical motion of the membrane. This is because membrane movement due to heating (in our case less than 1 °C) would lead to a different force-distance relationship for both electrostatic force and the Casimir force in disagreement with our observation and the confirmation of the distance independence of V_0 and V_0^l. The temperature rise of less than 1 °C is estimated based on the net thermal energy increase in the Si membrane. The absorption of photons during the course of the optical pulse increases the thermal energy of the membrane, while conductive and radiative heat outflow to the Si around the membrane and surroundings leads to a decrease in its thermal energy. The net change results in less than 1 °C. The latter would lead to a negligible, less than 10^{-6} relative expansion in the diameter of the membrane.

In order to account for roughness, the surface topography of the sphere and membrane was characterized using the AFM. Images resulting from the surface scan of the gold coating on the sphere demonstrate stochastically distributed roughness peaks with heights up to 32 nm. Table I contains the fractions v_k of the gold coating with heights h_k ($k=1,2,\ldots,33$). The surface scan of the Si surface demonstrates much smoother relief with maximum heights equal to

TABLE I. Fractions v_k of Au surface covered by roughness with heights h_k.

k	h_k (nm)	v_k
1	0	7×10^{-5}
2	1	6.0×10^{-4}
3	2	6.3×10^{-4}
4	3	7.0×10^{-4}
5	4	5.0×10^{-4}
6	5	2.1×10^{-3}
7	6	1.4×10^{-3}
8	7	4.0×10^{-3}
9	8	7.0×10^{-3}
10	9	8.0×10^{-3}
11	10	1.2×10^{-2}
12	11	1.3×10^{-2}
13	12	1.3×10^{-2}
14	13	2.0×10^{-2}
15	14	2.7×10^{-2}
16	15	3.6×10^{-2}
17	16	4.4×10^{-2}
18	17	6.0×10^{-2}
19	18	7.4×10^{-2}
20	19	8.6×10^{-2}
21	20	8.7×10^{-2}
22	21	8.8×10^{-2}
23	22	0.111
24	23	0.1
25	24	7.7×10^{-2}
26	25	5.4×10^{-2}
27	26	3.5×10^{-2}
28	27	2.0×10^{-2}
29	28	9.0×10^{-3}
30	29	4.0×10^{-3}
31	30	3.0×10^{-3}
32	31	1.0×10^{-3}
33	32	1.0×10^{-3}

1.68 nm. The fractions v_l of the Si surface with heights h_l ($l=1,2,\ldots,17$) are presented in Table II. The roughness data are used in Sec. IV in theoretical computations.

TABLE II. Fractions v_l of Si surface covered by roughness with heights h_l.

l	h_l (nm)	v_l
1	0	5.0×10^{-4}
2	0.18	1.5×10^{-3}
3	0.28	2.0×10^{-3}
4	0.38	4.0×10^{-3}
5	0.48	7.0×10^{-3}
6	0.58	5.0×10^{-3}
7	0.68	1.0×10^{-2}
8	0.78	4.0×10^{-2}
9	0.88	8.0×10^{-2}
10	0.98	0.15
11	1.08	0.22
12	1.18	0.215
13	1.28	0.147
14	1.38	8.3×10^{-2}
15	1.48	2.4×10^{-2}
16	1.58	9.0×10^{-3}
17	1.68	2.0×10^{-3}

IV. COMPARISON OF THE EXPERIMENTAL RESULTS WITH THE THEORY

A. Calculation of the Casimir force difference

The Casimir force acting between a large gold sphere of radius R and a plane Si membrane can be calculated by means of the Lifshitz formula,[29,30,60] along with the use of the proximity force theorem[34–38]

$$F_C(z)=k_BTR\sum_{l=0}^{\infty}{}'\left(1-\frac{1}{2}\delta_{l0}\right)\times\int_0^\infty k_\perp dk_\perp\{\ln[1-r_\parallel^{(1)}(\xi_l,k_\perp)r_\parallel^{(2)}(\xi_l,k_\perp)e^{-2q_lz}]+\ln[1-r_\perp^{(1)}(\xi_l,k_\perp)r_\perp^{(2)}(\xi_l,k_\perp)e^{-2q_lz}]\}. \quad (10)$$

Here, k_B is the Boltzmann constant. The reflectivity coefficients for gold ($k=1$) and Si ($k=2$) for the two independent polarizations of electromagnetic field (transverse magnetic and transverse electric modes) are defined by

$$r_\parallel^{(k)}(\xi_l,k_\perp)=\frac{\varepsilon_l^{(k)}q_l-k_l^{(k)}}{\varepsilon_l^{(k)}q_l+k_l^{(k)}},\quad r_\perp^{(k)}(\xi_l,k_\perp)=\frac{k_l^{(k)}-q_l}{k_l^{(k)}+q_l}, \quad (11)$$

where $\xi_l=2\pi k_BTl/\hbar$ are the Matsubara frequencies, $\varepsilon_l^{(k)}=\varepsilon^{(k)}(i\xi_l)$, $\varepsilon^{(k)}(\omega)$ are the frequency-dependent dielectric permittivities of gold and Si, and the following notations are introduced:

$$q_l=\left(\frac{\xi_l^2}{c^2}+k_\perp^2\right)^{1/2},\quad k_l^{(k)}=\left[\varepsilon^{(k)}(i\xi_l)\frac{\xi_l^2}{c^2}+k_\perp^2\right]^{1/2}. \quad (12)$$

The dielectric permittivities of gold and of high-resistivity Si in the absence of laser light were computed[18,61] by means of the dispersion relation

$$\varepsilon^{(k)}(i\xi)=1+\frac{2}{\pi}\int_0^\infty d\omega\frac{\omega\,\mathrm{Im}\,\varepsilon^{(k)}(\omega)}{\omega^2+\xi^2}, \quad (13)$$

where $\mathrm{Im}\,\varepsilon^{(k)}(\omega)$ are taken from the tabulated optical data for the complex index of refraction.[52] High-precision results for $\varepsilon^{(1)}(i\xi)$ (gold) are presented in Ref. 61. For high-resistivity

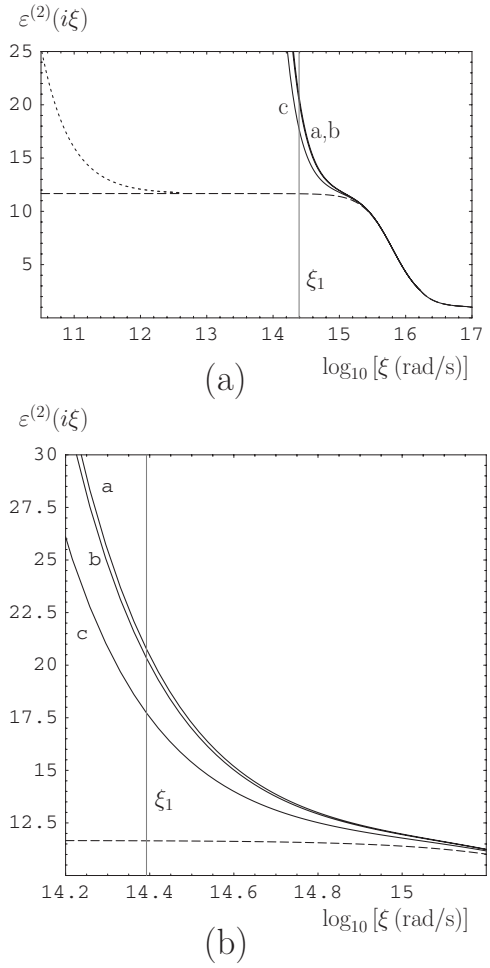

FIG. 7. (a) The dielectric permittivity of the Si membrane along the imaginary frequency axis in the absence of light (the long-dashed line is for the model of Si with a finite static permittivity and the short-dashed line includes dc conductivity of high-resistivity Si) and in the presence of light for different absorbed powers [solid lines: *a*, 9.3 mW; *b*, 8.5 mW; and *c*, 4.7 mW]. (b) The same is shown on an enlarged scale in the region of the first Matsubara frequency ξ_1.

Si, the behavior of $\varepsilon^{(2)}(i\xi)$ as a function of ξ is shown by the long-dashed line in Figs. 7(a) and 7(b). In particular, $\varepsilon^{(2)}(0)\approx 11.66$.

On irradiation of the Si membrane by light, the equilibrium value of the carrier density is rapidly established during a period of time much shorter than the duration of the laser pulse. Therefore, we assume that there is an equilibrium concentration of pairs (electrons and holes) when the light is incident. Thus, in the presence of laser radiation, the dielectric permittivity of Si along the imaginary frequency axis can be represented in the commonly used form[43–45,47,49,52]

$$\varepsilon_l^{(2)}(i\xi)=\varepsilon^{(2)}(i\xi)+\frac{\omega_p^{(e)2}}{\xi[\xi+\gamma^{(e)}]}+\frac{\omega_p^{(p)2}}{\xi[\xi+\gamma^{(p)}]}, \tag{14}$$

where $\omega_p^{(e,p)}$ and $\gamma^{(e,p)}$ are the plasma frequencies and the relaxation parameters for electrons and holes, respectively.

The values of the relaxation parameters $\gamma^{(e)}\approx 1.8\times 10^{13}$ rad/s and $\gamma^{(p)}\approx 5.0\times 10^{12}$ rad/s can be found in Ref. 47. The plasma frequencies can be calculated from

$$\omega_p^{(e,p)}=\left(\frac{ne^2}{m_{e,p}^*\varepsilon_0}\right)^{1/2}, \tag{15}$$

where the effective masses are[47] $m_p^*=0.2063m_e$ and $m_e^*=0.2588m_e$, m_e is the electron mass, and n is the concentration of charge carriers.

The value of n for the different absorbed powers can be calculated in the following way. First, we note that for a membrane of $d=4$ μm thickness, n does not depend on the depth. The reason is that a uniform concentration in this direction is established even more rapidly than the equilibrium discussed above.[47] In fact, the assumption on a uniform charge-carrier density in the Si membrane is justified due to the long carrier diffusion lengths and the ability to obtain almost defect-free surfaces in silicon through hydrogen passivation.[62] Next, we approximately model the central part of the Gaussian beam of diameter w by a uniform cylindrical beam of the same diameter. The power contained in this cylindrical beam, P_w^{eff}, is equal to the power in the central part of the Gaussian beam with a diameter w. Elementary calculation using the Gaussian distribution leads to $P_w^{\mathrm{eff}}=0.393P^{\mathrm{eff}}$. The power P_w^{eff} is absorbed uniformly in the central part of the Si membrane of diameter w having a volume $V=\pi w^2 d/4$. Incidentally, the central region of the membrane with a diameter w contributes almost 100% [99.9999% (Ref. 63)] of the total Casimir force acting between a membrane and a sphere. At equilibrium, the number of created charge-carrier pairs per unit time per unit volume $P_w^{\mathrm{eff}}/(\hbar\omega V)$, where $\omega=3.66\times 10^{15}$ rad/s is the frequency of Ar laser light, is equal to the recombination rate of pairs per unit volume n/τ. Thus, at equilibrium

$$n=\frac{4P_w^{\mathrm{eff}}\tau}{\hbar\omega d\pi w^2}. \tag{16}$$

Equations (15) and (16) allow us to calculate the densities of charge carriers $n_a=(2.1\pm 0.4)\times 10^{19}$ cm^{-3}, $n_b=(2.0\pm 0.4)\times 10^{19}$ cm^{-3}, and $n_c=(1.4\pm 0.3)\times 10^{19}$ cm^{-3} and the respective plasma frequencies

$$\begin{aligned}
\omega_{p,a}^{(e)}&=(5.1\pm 0.5)\times 10^{14}\ \mathrm{rad/s},\\
\omega_{p,a}^{(p)}&=(5.7\pm 0.6)\times 10^{14}\ \mathrm{rad/s},\\
\omega_{p,b}^{(e)}&=(5.0\pm 0.5)\times 10^{14}\ \mathrm{rad/s},\\
\omega_{p,b}^{(p)}&=(5.6\pm 0.5)\times 10^{14}\ \mathrm{rad/s},\\
\omega_{p,c}^{(e)}&=(3.7\pm 0.4)\times 10^{14}\ \mathrm{rad/s},\\
\omega_{p,c}^{(p)}&=(4.1\pm 0.4)\times 10^{14}\ \mathrm{rad/s}
\end{aligned} \tag{17}$$

in all measurements *a*, *b*, and *c* with different powers of the absorbed laser light. In the calculations of charge-carrier densities using Eq. (16), we have used $\tau_a=\tau_b=0.38\pm 0.03$ ms and $\tau_c=0.47\pm 0.01$ ms in accordance with the measurement results in Sec. III B, taking into account the fact that τ decreases when n increases. Recall that τ_a and τ_b

were obtained from the first 0.5 ms of the time decay. Our value for τ_c obtained using the whole 5 ms decay may lead to a minor underestimation of the carrier density, a fact included in the resulting 21% error in the value of n_c. Note that the above values of the relaxation parameters $\gamma^{(e)}$ and $\gamma^{(p)}$ do not depend on the absorbed power[47] and can be used in all measurements.

In Fig. 7(a), the dielectric permittivity of Si in the presence of laser radiation [Eq. (14)] is shown by solid lines *a*, *b*, and *c* as a function of imaginary frequency for the measurements with different absorbed powers *a*, *b*, and *c*, respectively. The lines *a* and *b* in Fig. 7(a) almost coincide. The region around the first Matsubara frequency ξ_1 at $T=300$ K is shown in Fig. 7(b) on an enlarged scale.

The obtained values of $\varepsilon^{(1)}(i\xi)$, $\varepsilon^{(2)}(i\xi)$, and $\varepsilon_l^{(2)}(i\xi)$ were substituted in the Lifshitz formula (10), and the difference of the Casimir forces $\Delta F_C(z)$ from Eq. (5) in the presence and in the absence of laser light was computed at the laboratory temperature $T=300$ K. Note that there is a discussion in the literature on the correct value of the reflection coefficient for gold $r_\perp^{(1)}(0,k_\perp)$ at zero frequency (see, e.g., Refs. 17–19 and 64–67). Our calculation, however, does not depend on the chosen value of $r_\perp^{(1)}(0,k_\perp)$ because in Eq. (10) it is multiplied by $r_\perp^{(2)}(0,k_\perp)=0$ for the silicon. In the absence of light, the latter equality holds for any true dielectric with finite static dielectric permittivity. In the presence of light, the equality $r_{\perp,l}^{(2)}(0,k_\perp)=0$ also holds true as is seen from the substitution of Eq. (14) into Eq. (11). In both cases, at zero frequency only the transverse magnetic mode of the electromagnetic field contributes to the result. Note that for Si in the absence and in the presence of light for the transverse magnetic mode,

$$r_\parallel^{(2)}(0,k_\perp)=\frac{\varepsilon^{(2)}(0)-1}{\varepsilon^{(2)}(0)+1} \qquad \text{and} \qquad r_{\parallel,l}^{(2)}(0,k_\perp)=1, \tag{18}$$

respectively. Finally, the Lifshitz formula (10) was used to compute the difference in the Casimir forces at all experimental separations z_i $(1\leqslant i\leqslant 1209)$ and for the three measurements performed at different absorbed powers.

The results of these calculations should be corrected for the presence of surface roughness.[68] The stochastic roughness on our test bodies can be taken into account using the procedure presented in detail in Refs. 18, 24, 43, and 44. First, the zero roughness levels on both gold $(H_0^{(1)})$ and Si $(H_0^{(2)})$ are determined from

$$\sum_{k=1}^{33}(H_0^{(1)}-h_k)v_k=\sum_{l=1}^{17}(H_0^{(2)}-h_l)v_l=0, \tag{19}$$

where the heights h_k, h_l and the fractions of the surfaces covered by roughness with these heights are given in Tables I and II, respectively. From Eq. (19), it follows that $H_0^{(1)}=20.0$ nm and $H_0^{(2)}=1.1$ nm. The absolute separation z between the test bodies is, in fact, measured between the zero roughness levels. Then, the theoretical values of the difference Casimir force with account of the surface roughness are calculated as the geometric averaging

$$\Delta F_C^{\text{theor}}(z_i)=\sum_{k=1}^{33}\sum_{l=1}^{17}v_kv_l\Delta F_C(z_i+H_0^{(1)}+H_0^{(2)}-h_k-h_l), \tag{20}$$

where $\Delta F_C(z)$ was computed by the Lifshitz formula for perfectly shaped bodies with and without light on a Si membrane. In the present experiments, the contribution from roughness correction is very small. Thus, at $z=100$ nm, it contributes only 1.2% of the calculated $\Delta F_C^{\text{theor}}(z)$. At $z=150$ nm, the contribution from surface roughness decreases to only 0.5% of the calculated force difference. Similar to Refs. 18, 24, and 44, it is easily seen that the contribution from the nonadditive, diffraction-type effects to roughness correction [which is not taken into account in Eq. (20)] is negligibly small.

The results of the numerical computations of the difference Casimir force between rough surfaces $\Delta F_C^{\text{theor}}(z)$ are shown as solid lines in Figs. 5(a)–5(c) for the measurements with different powers of the absorbed laser light. They are in very good agreement with the experimental data shown by dots in the same figures (see the following sections for the quantitative measure of agreement between experiment and theory).

For completeness, we also present the results of theoretical computations using the Lifshitz formula at zero temperature. They are obtained from Eq. (10) by changing the discrete Matsubara frequencies ξ_l for continuous ξ and by replacement of the summation for integration,

$$k_BT\sum_{l=0}^{\infty}{}'\left(1-\frac{1}{2}\delta_{l0}\right)\to\frac{\hbar}{2\pi}\int_0^\infty d\xi. \tag{21}$$

Following the same procedure as at $T=300$ K, we first calculate $\Delta F_C(z;T=0)$ using the Lifshitz formula and then find $\Delta F_C^{\text{theor}}(z;T=0)$ including the effect of surface roughness with Eq. (20). The results of these computations are shown as short-dashed lines in Figs. 5(a)–5(c). As is seen in the figure, in all cases the short-dashed lines describe a slightly larger magnitude of the Casimir force difference than at $T=300$, in rather good agreement with the experimental data shown as dots (see the next sections for further discussion).

B. Analysis of theoretical errors

The theoretical errors in the computation of the Casimir force acting between a sphere and a membrane were discussed in detail in Refs. 24 and 44. The major source of the theoretical uncertainty in this experiment is the error in the concentration of charge carriers n when the light is on. From Sec. IV A, this error is of about 20%. Calculations using the Lifshitz formula show that the resulting relative error in the difference Casimir force, $\delta_1(\Delta F_C^{\text{theor}})\approx 0.12$, i.e., is equal to approximately 12% and does not depend on separation. The error due to uncertainty of experimental separations z_i, in which the theoretical values $\Delta F_C^{\text{theor}}$ should be computed, is equal to $3\Delta z/z$ and takes the maximum value of 3% of the

Casimir force at the shortest separation of $z=100$ nm (recall that according to Sec. III A $\Delta z=1$ nm). This leads to only 2% error in the difference of the Casimir force at $z=100$ nm [so that $\delta_2(\Delta F_C^{\text{theor}})\approx 0.02$] and to smaller errors at larger separations. The other sources of theoretical errors, discussed in Refs. 24 and 44, such as sample-to-sample variation of the tabulated optical data in Au, use of the proximity force theorem, patch potentials, nonlocal effects, and finite thickness of the gold coating on the sphere contribute negligible amounts to the error in $\Delta F_C^{\text{theor}}$. Thus, for example, using the Lifshitz formula for a polystyrene sphere covered by a gold layer of 82 nm thickness instead of Eq. (10) written for a solid gold sphere, we would get only a 0.03% decrease in the Casimir force magnitude.

A specific uncertainty which is present in this experiment is connected with the pressure of light transmitted through the membrane and incident on the bottom of the sphere (see Sec. II). This effect is present only during the light phase of the pulse train and can be easily estimated. The maximum intensity of the laser light incident on a sphere section with radius $0\leqslant r\leqslant R$ parallel to the membrane is

$$I(r)=\frac{2\alpha P^{\text{eff}}}{\pi w^2}e^{-2r^2/w^2}, \tag{22}$$

where α is the fraction of the absorbed power transmitted through the membrane. The value of α is given by

$$\alpha=re^{-d/l_{\text{opt}}}\approx 0.006\,41, \tag{23}$$

where $l_{\text{opt}}=1$ μm (see Sec. II) and the transmission coefficient $r\approx 0.35$.

The force due to light pressure acting on the sphere in spherical coordinates takes the form

$$F_p=\frac{4\pi R^2}{c}\int_0^{\pi/2}d\vartheta I(R\sin\vartheta)\cos^2\vartheta\sin\vartheta. \tag{24}$$

Substituting Eq. (22) into Eq. (24) and integrating, one obtains

$$F_p=\frac{2\alpha P^{\text{eff}}}{c}\left[1-e^{-2R^2/w^2}\frac{\sqrt{\pi}w\,\text{Erfi}(\sqrt{2}R/w)}{2\sqrt{2}R}\right], \tag{25}$$

where Erfi(z) is the imaginary error function.

For the absorbed powers used in three experiments ($P^{\text{eff}}=9.3$, 8.5, and 4.7 mW, respectively), Eq. (25) leads to the following maximum forces which may act on the sphere due to light pressure: $F_p=0.085$, 0.078, and 0.043 pN. The force due to light pressure can be taken into account as one more error in the theoretical evaluation of the Casimir force difference $\Delta F_C^{\text{theor}}$. At a separation $z=100$ nm, the respective relative error, $\delta_3(\Delta F_C^{\text{theor}})$, is equal to 2.3%, 2.7%, and 1.5% for the three absorbed powers. At $z=200$ nm, the relative theoretical error in $\Delta F_C^{\text{theor}}$ due to light pressure increases up to 8.9%, 8.7%, and 5.0%, respectively.

All three errors discussed above can be considered as the random quantities described by the same distribution law which is close to a uniform distribution. For this reason, the statistical criterion[58] used in Sec. III C can be applied once more, giving the total relative theoretical error in the difference Casimir force,

$$\delta^{\text{tot}}(\Delta F_C^{\text{theor}})=\min\left\{\sum_{i=1}^{q}\delta_i(\Delta F_C^{\text{theor}}),k_\beta^{(q)}\sqrt{\sum_{i=1}^{q}[\delta_i(\Delta F_C^{\text{theor}})]^2}\right\}, \tag{26}$$

with $q=3$ and $k_{0.95}^{(3)}=1.12$. The resulting total absolute theoretical error,

$$\Delta^{\text{tot}}(\Delta F_C^{\text{theor}})=|\Delta F_C^{\text{theor}}|\delta^{\text{tot}}(\Delta F_C^{\text{theor}}), \tag{27}$$

is presented in Fig. 8 as a function of separation for the three experiments with decreasing power of the absorbed laser light (lines a, b, and c, respectively). As is seen in this figure, the total theoretical errors for measurements a and b are almost equal, and for measurement c this error is slightly lower. The relative total theoretical error changes from 13.5% to 13.7% at $z=100$ nm and from 13.7% to 14.4% at $z=140$ nm for the three different absorbed powers. At $z=200$ nm, the relative total theoretical error ranges from 14.9% to 17.2% for the different absorbed powers.

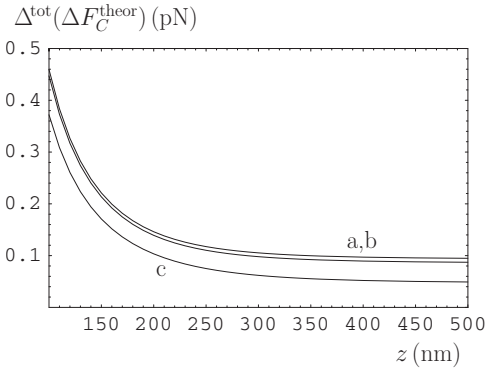

FIG. 8. The total theoretical errors versus separation for measurements with different absorbed powers: a, 9.3 mW; b, 8.5 mW; and c, 4.7 mW.

C. Measure of agreement between experiment and theory

In the foregoing sections, we have independently found the total experimental (Sec. III C) and theoretical (Sec. IV B) errors in the difference of the Casimir force in the presence and in the absence of laser light excited carriers at 95% confidence. To compare experiment with theory, we consider the quantity $\Delta F_C^{\text{theor}}-\Delta F_C^{\text{expt}}$ and determine its absolute error $\Xi_{0.95}(z)$ as a function of separation at the confidence of 95%. This can be done in the same procedure as in Refs. 18, 44, and 59 applying the statistical criterion[58] and using the data in Figs. 6 and 8,

$$\Xi_\beta=\min\{\Delta^{\text{tot}}(\Delta F_C^{\text{expt}})+\Delta^{\text{tot}}(\Delta F_C^{\text{theor}}),k_\beta^{(2)}\sqrt{[\Delta^{\text{tot}}(\Delta F_C^{\text{expt}})]^2+[\Delta^{\text{tot}}(\Delta F_C^{\text{theor}})]^2}\}. \tag{28}$$

Here, $k_{0.95}^{(2)}=1.10$. The resulting confidence intervals

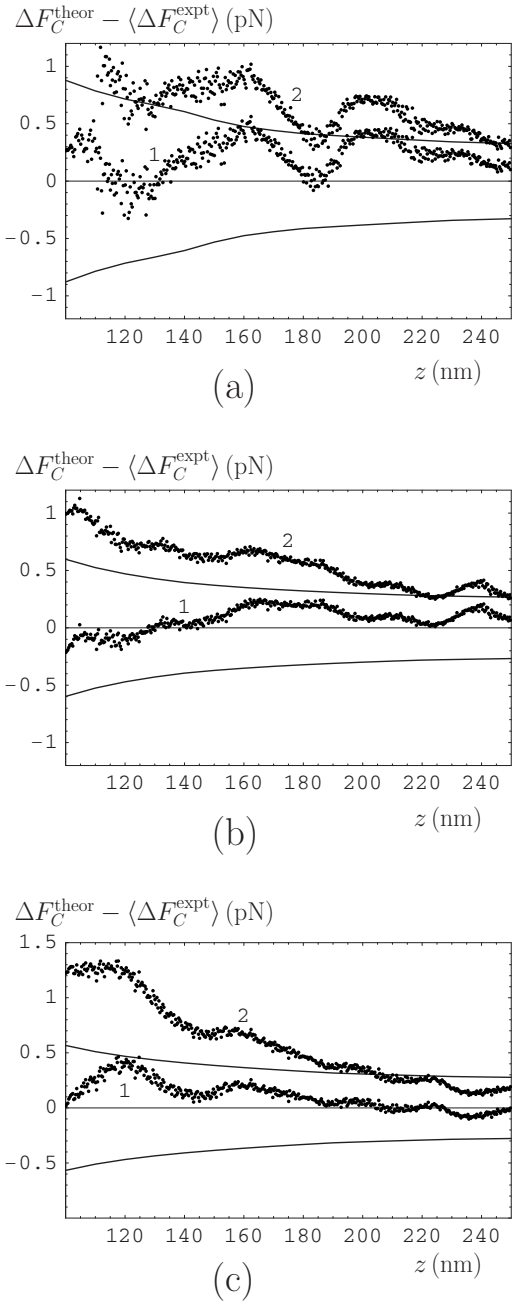

FIG. 9. Theoretical minus experimental differences in the Casimir force versus separation for the measurements with different absorbed powers, (a) 9.3 mW, (b) 8.5 mW, and (c) 4.7 mW, are shown as dots. The results computed at $T=300$ K using the model with a finite static permittivity of high-resistivity Si are labeled 1 and those including the dc conductivity are labeled 2. Solid lines show the 95% confidence intervals.

$[-\Xi_{0.95}(z), \Xi_{0.95}(z)]$ are shown in Figs. 9(a)–9(c) as the solid lines for the three measurements with the largest, intermediate, and smallest powers, respectively.

The differences between the theoretical values of $\Delta F_C^{\rm theor}$ (computed in Sec. IV A at $T=300$ K) and experimentally measured $\langle \Delta F_C^{\rm expt} \rangle$ are shown in Fig. 9 by dots labeled 1 (once again, dots in Figs. 9(a)–9(c) are related to the three measurements with different powers). As seen in Fig. 9,

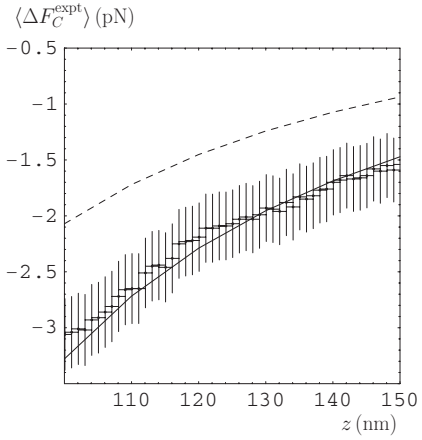

FIG. 10. The experimental differences in the Casimir force with their experimental errors are shown as crosses. Solid and dashed lines represent the theoretical differences computed at $T=300$ K using the model with a finite static permittivity of high-resistivity Si and that including the dc conductivity, respectively.

practically all dots labeled 1 are well inside the confidence intervals at all separation distances. This means that the Lifshitz theory at nonzero temperature, using the dielectric permittivity of high-resistivity Si $\varepsilon^{(2)}(i\xi)$ in the absence of laser light and the dielectric permittivity $\varepsilon_l^{(2)}(i\xi)$ given by Eq. (14) in the presence of light, is consistent with experiment. The consistency of the experiment with the theory is preserved when the theoretical values of $\Delta F_C^{\rm theor}$ are computed at zero temperature [see the short-dashed lines in Figs. 5(a)–5(c) and the discussion in Sec. IV A]. The reason is that the thermal correction to the Casimir force in the region of small separations under consideration is practically negligible and the thermal effect cannot be resolved taking into consideration the experimental and theoretical errors reported above.

For illustrative purposes, the agreement between experiment and theory is presented in a more standard form in Fig. 10. Here, a more narrow separation interval from 100 to 150 nm is considered and each third experimental point from the measurement b is plotted together with its error bars $[\pm\Delta z, \pm\Delta^{\rm tot}(\Delta F_C^{\rm expt})]$ shown as crosses (there are too many points to present all of them in this form). The theoretical force difference $\Delta F_C^{\rm theor}$ computed by the Lifshitz formula at $T=300$ K is shown by the solid line. It is seen that the experimental data are in very good agreement with the theory, in confirmation of the conclusion made above using Fig. 9.

V. PROBLEM OF dc CONDUCTIVITY OF HIGH-RESISTIVITY Si IN THE LIFSHITZ THEORY

In Sec. IV A, the dielectric response of high-resistivity Si in the absence of excitation laser light was described by the function $\varepsilon^{(2)}(i\xi)$ having a finite static value $\varepsilon^{(2)}(0)\approx 11.66$. It is common knowledge, however, that dielectrics have some nonzero dc conductivity σ_0 at any nonzero temperature. This conductivity decreases with the decrease of temperature as $\sigma_0 \sim \exp(-b/T)$, where b can be expressed in terms of the

band gap or dopant activation energy. To take the dc conductivity into account in the Lifshitz theory, the dielectric permittivity of Si along the imaginary frequency axis $\varepsilon^{(2)}(i\xi)$ used in Sec. IV A should be replaced with

$$\tilde{\varepsilon}^{(2)}(i\xi) = \varepsilon^{(2)}(i\xi) + \frac{\tilde{\omega}_p^{(p)2}}{\xi[\xi + \gamma^{(p)}]}. \tag{29}$$

The value of the plasma frequency in Eq. (29) is found by substituting the concentration of carrier density $\tilde{n} \approx 5 \times 10^{14}$ cm^{-3} (see Sec. II) into Eq. (15) with the result $\tilde{\omega}_p^{(p)} \approx 2.8 \times 10^{12}$ rad/s. Note that for $n \leqslant 1.0 \times 10^{17}$ cm^{-3}, the value of the relaxation parameter has an insignificant effect on the magnitude of the Casimir force.[47] Because of this, in Eq. (29) the same value of $\gamma^{(p)}$ as in Eq. (14) is used. The behavior of $\tilde{\varepsilon}^{(2)}$ as a function of ξ is plotted in Fig. 7(a) by the short-dashed line.

The presence of some low dc conductivity in dielectric materials was used in Refs. 7 and 69 to obtain a large effect of the van der Waals friction which could bring the observations of Ref. 6 in agreement with theory. In Ref. 8 for two dielectric plates and in Refs. 50 and 51 for one metal and one dielectric plate, it was proved, however, that the inclusion of the dc conductivity for dielectrics into the Lifshitz theory leads to the violation of the third law of thermodynamics (the Nernst heat theorem). Thus, it is not acceptable from a theoretical point of view.

Our experiments on the modification of the Casimir force with laser pulses clarify the problem whether or not the dc conductivity of high-resistivity Si should be taken into account in the Lifshitz theory of the Casimir and van der Waals forces. For this purpose, we have completely repeated the theoretical computations of the difference Casimir force made in Sec. IV A, replacing the dielectric permittivity of Si $\varepsilon^{(2)}(i\xi)$, used there, for $\tilde{\varepsilon}^{(2)}(i\xi)$ given in Eq. (29). The obtained theoretical results for $\Delta\tilde{F}_C^{\text{theor}}$ versus separation are shown by the long-dashed lines in Figs. 5(a)–5(c) for all the three measurements with different powers of the absorbed light. As is seen in Fig. 5, all the long-dashed lines are far outside both the experimental data shown as dots and from the solid lines calculated using the Lifshitz theory disregarding dc conductivity of high-resistivity Si at the laboratory temperature. Notice that the computational results at $T=0$ (shown by the short-dashed lines in Fig. 5) do not depend on whether the dc conductivity is included in the dielectric permittivity used to describe the high-resistivity Si.

To make a quantitative conclusion on the measure of agreement between the data and two models with and without inclusion of dc conductivity of high-resistivity Si, we have plotted in Figs. 9(a)–9(c) the differences $\Delta\tilde{F}_C^{\text{theor}} - \langle \Delta F_C^{\text{expt}} \rangle$, where $\Delta\tilde{F}_C^{\text{theor}}$ was computed including the dc conductivity according to Eq. (29). These differences are shown as dots labeled 2 in Figs. 9(a)–9(c). As is seen in Figs. 9(a) and 9(b), the model with included dc conductivity of high-resistivity Si is excluded experimentally at 95% confidence within the region from 100 to 250 nm. In Fig. 9(c), it follows that this model is excluded at 95% confidence within the separation region from 100 to 200 nm.

The same conclusion, that the model of high-resistivity Si, which includes dc conductivity, is inconsistent with our experiments on the optically modulated Casimir force, is confirmed also in Fig. 10, where the quantity $\Delta\tilde{F}_C^{\text{theor}}$ versus separation is plotted as the dashed line. It can be clearly observed that the dashed line is not only far away from the solid line based on theory neglecting the Si dc conductivity in the absence of excitation light but also distant from all error bars representing the experimental data.

The physical explanation for the deviations of the long-dashed lines from the solid lines in Figs. 5(a)–5(c) and 10 is as follows. When the dc conductivity of Si is taken into account, the equalities $r_\perp^{(2)}(0,k_\perp) = r_{\perp,l}^{(2)}(0,k_\perp) = 0$ follow from the substitution of Eqs. (14) and (29) into Eq. (11). Once again, at zero frequency only the transverse magnetic mode contributes to the result. Here, however, for Si both in the absence and in the presence of light the equations

$$\tilde{r}_\parallel^{(2)}(0,k_\perp) = 1 \qquad \text{and} \qquad \tilde{r}_{\parallel,l}^{(2)}(0,k_\perp) = 1 \tag{30}$$

hold. It is exactly this change in the magnitude of the transverse magnetic reflection coefficient $r_\parallel^{(2)}(0,k_\perp)$, as given in Eq. (18), with $\tilde{r}_\parallel^{(2)}(0,k_\perp)$ in Eq. (30) that leads to the deviation of the long-dashed lines from the respective solid lines in Figs. 5(a)–5(c) and 10. It seems somewhat surprising that the use of the permittivity $\tilde{\varepsilon}^{(2)}(i\xi)$ in Eq. (29), which can be considered as more exact than $\varepsilon^{(2)}(i\xi)$, leads to the discrepancy between experiment and theory. This is, in fact, one more observation that there are puzzles concerning the applicability of the Lifshitz theory to real materials. In the case of metals, the Drude description of conduction electrons in the thermal Casimir force was excluded experimentally in a series of experiments.[17–19] It also leads to the contradiction with the Nernst heat theorem for perfect crystal lattices.[66] For metals, the deviation of the experimental results from the Drude model approach and the violation of the Nernst theorem are explained by the vanishing contribution from the transverse electric mode at zero frequency. The present experiment dealing with semiconductors is not sensitive enough to detect this effect. The effect reported here arises due to the difference in the contributions of the zero-frequency transverse magnetic mode. These contributions, as were shown above, depend on whether or not the dc conductivity of Si in the absence of light is taken into account.

VI. CONCLUSIONS AND DISCUSSION

In this paper, we demonstrate that it is possible to control the Casimir force between the gold coated sphere and the Si membrane by the irradiation of Si with laser pulses. On absorption of light, the carrier density increases, leading to an increase in the magnitude of the Casimir force. This change in the Casimir forces was investigated as a function of separation between the test bodies and the power of the absorbed light. The experiments were performed with a specially prepared single-crystal Si membrane in an oil-free vacuum chamber using an AFM. The developed calibration procedure permitted measurement of the difference Casimir force of the order of 1 pN with a relative experimental error at the short-

est separation of 100 nm varying from 10% to 20% for the measurements performed at different absorbed powers. At a separation of 180 nm, the relative experimental error in different measurements varies from 25% to 33%. All errors were determined at 95% confidence. The obtained experimental results demonstrate the ability to modulate the van der Waals and Casimir forces in micro- and nanoelectromechanical devices by irradiation with laser light. These are experiments where the modification of the Casimir force acting between the test bodies was achieved due to the influence of some external factor other than the change of separation distance.

The experimental results were compared with the results of theoretical computations using the Lifshitz theory at both zero and nonzero temperature. The Si membrane in the absence of laser light had a carrier density of approximately 5×10^{14} cm^{-3}. In the first model, the dielectric permittivity of high-resistivity Si was described with a finite static value. In the presence of laser light, the Si had charge-carrier pair densities varying from 2.1×10^{19} to 1.4×10^{19} cm^{-3} depending on the radiation power absorbed by the sample and was described by the permittivity in Eq. (14). The total theoretical error varied from 13.5% to 13.7% at $z=100$ nm and from 14.9% to 17.2% at $z=200$ nm depending on the absorbed power. The main contribution to this error was given by the uncertainty in the number of charge carriers in the presence of laser light. The experimental and theoretical results were found to be consistent over the whole measurement range taking into account the experimental and theoretical errors both at laboratory temperature $T=300$ K and at zero temperature.

The same experimental data were compared with the Lifshitz theory using a second model of high-resistivity Si which includes the dc conductivity of the Si membrane in the absence of laser radiation. In this case, the dielectric permittivity of Si in the absence of radiation is represented by Eq. (29) and goes to infinity when the frequency goes to zero. The detailed comparison leads to the conclusion that this model is excluded by the experiment at 95% confidence if computations are performed at the laboratory temperature $T=300$ K. The difference in the force magnitudes when conductivity at zero frequency is absent or present arises from different contributions of the transverse magnetic modes of the electromagnetic field reflected from the Si surface. The physical explanation of our results can be understood in Fig. 7(a). As is seen in this figure, the short-dashed line representing the dielectric permittivity of high-resistivity Si with included dc conductivity is located far to the left of the first Matsubara frequency ξ_1 and does not belong to the region of frequencies contributing to the force. At the same time, the Lifshitz theory at zero temperature using the model of high-resistivity Si with included dc conductivity remains experimentally consistent.

Thus, we can infer that the Lifshitz theory at nonzero temperature using the model of high-resistivity semiconductors and dielectrics with included conductivity properties at zero frequency is inconsistent with our experiments. It is notable that just this theoretical approach was demonstrated[8,50,51,70] to lead to the violation of the third law of thermodynamics (the Nernst heat theorem). To avoid contradictions with thermodynamics and experiment, one should follow the originators of the Lifshitz theory[29,30] who described dielectrics by a model with a finite static dielectric permittivity in computations of the van der Waals and Casimir forces at nonzero temperature (the same model was used in the recent paper[71] on the thermal effect in the Casimir-Polder force). This suggests that the theory of van der Waals and Casimir forces between real materials requires further investigation. Although we are still lacking a fundamental explanation of why the Lifshitz theory does not admit inclusion of the conductivity properties of high-resistivity materials at zero frequency, this prescription on how to perform computations in an experimentally and thermodynamically consistent way is topical for numerous applications of the van der Waals and Casimir forces ranging from condensed matter physics and nanotechnology to the theory of fundamental interactions. The experimentally demonstrated phenomenon of modulation of the Casimir force through optical modification of charge-carrier density will be used in the design and function of micro- and nanoelectromechanical devices such as nanoscale actuators, micromirrors, and nanotweezers.

ACKNOWLEDGMENTS

G.L.K. and V.M.M. are grateful to the Department of Physics and Astronomy of the University of California (Riverside). The instrumentation in this work was supported by NSF Grant No. PHY0653657. Theoretical calculations and personnel were supported by DOE Grant No. DE-FG02-04ER46131.

[1] H. B. G. Casimir, Proc. K. Ned. Akad. Wet. **51**, 793 (1948).
[2] E. Buks and M. L. Roukes, Phys. Rev. B **63**, 033402 (2001).
[3] H. B. Chan, V. A. Aksyuk, R. N. Kleiman, D. J. Bishop, and F. Capasso, Science **291**, 1941 (2001); Phys. Rev. Lett. **87**, 211801 (2001).
[4] A. A. Chumak, P. W. Milonni, and G. P. Berman, Phys. Rev. B **70**, 085407 (2004).
[5] M. Kardar and R. Golestanian, Rev. Mod. Phys. **71**, 1233 (1999).
[6] B. C. Stipe, H. J. Mamin, T. D. Stowe, T. W. Kenny, and D. Rugar, Phys. Rev. Lett. **87**, 096801 (2001).
[7] J. R. Zurita-Sánchez, J.-J. Greffet, and L. Novotny, Phys. Rev. A **69**, 022902 (2004).
[8] B. Geyer, G. L. Klimchitskaya, and V. M. Mostepanenko, Phys. Rev. D **72**, 085009 (2005).
[9] G. Barton, J. Phys. A **37**, 1011 (2004); **38**, 2997 (2005).
[10] E. V. Blagov, G. L. Klimchitskaya, and V. M. Mostepanenko, Phys. Rev. B **71**, 235401 (2005).
[11] M. Bordag, B. Geyer, G. L. Klimchitskaya, and V. M. Mostepanenko, Phys. Rev. B **74**, 205431 (2006).
[12] E. V. Blagov, G. L. Klimchitskaya, and V. M. Mostepanenko, Phys. Rev. B **75**, 235413 (2007).
[13] M. Antezza, L. P. Pitaevskii, and S. Stringari, Phys. Rev. A **70**,

053619 (2004).
[14] J. F. Babb, G. L. Klimchitskaya, and V. M. Mostepanenko, Phys. Rev. A **70**, 042901 (2004).
[15] M. Bordag, B. Geyer, G. L. Klimchitskaya, and V. M. Mostepanenko, Phys. Rev. D **58**, 075003 (1998); **60**, 055004 (1999); **62**, 011701(R) (2000).
[16] J. C. Long, H. W. Chan, and J. C. Price, Nucl. Phys. B **539**, 23 (1999).
[17] R. S. Decca, E. Fischbach, G. L. Klimchitskaya, D. E. Krause, D. López, and V. M. Mostepanenko, Phys. Rev. D **68**, 116003 (2003).
[18] R. S. Decca, D. López, E. Fischbach, G. L. Klimchitskaya, D. E. Krause, and V. M. Mostepanenko, Ann. Phys. (N.Y.) **318**, 37 (2005).
[19] R. S. Decca, D. López, E. Fischbach, G. L. Klimchitskaya, D. E. Krause, and V. M. Mostepanenko, Phys. Rev. D **75**, 077101 (2007).
[20] S. K. Lamoreaux, Phys. Rev. Lett. **78**, 5 (1997); **81**, 5475(E) (1998).
[21] U. Mohideen and A. Roy, Phys. Rev. Lett. **81**, 4549 (1998); G. L. Klimchitskaya, A. Roy, U. Mohideen, and V. M. Mostepanenko, Phys. Rev. A **60**, 3487 (1999).
[22] A. Roy and U. Mohideen, Phys. Rev. Lett. **82**, 4380 (1999).
[23] A. Roy, C.-Y. Lin, and U. Mohideen, Phys. Rev. D **60**, 111101(R) (1999).
[24] B. W. Harris, F. Chen, and U. Mohideen, Phys. Rev. A **62**, 052109 (2000); F. Chen, G. L. Klimchitskaya, U. Mohideen, and V. M. Mostepanenko, *ibid.* **69**, 022117 (2004).
[25] G. Bressi, G. Carugno, R. Onofrio, and G. Ruoso, Phys. Rev. Lett. **88**, 041804 (2002).
[26] F. Chen, U. Mohideen, G. L. Klimchitskaya, and V. M. Mostepanenko, Phys. Rev. Lett. **88**, 101801 (2002); Phys. Rev. A **66**, 032113 (2002).
[27] M. Bordag, U. Mohideen, and V. M. Mostepanenko, Phys. Rep. **353**, 1 (2001).
[28] S. K. Lamoreaux, Rep. Prog. Phys. **68**, 201 (2005).
[29] E. M. Lifshitz, Zh. Eksp. Teor. Fiz. **29**, 94 (1956); [Sov. Phys. JETP **2**, 73 (1956)].
[30] E. M. Lifshitz and L. P. Pitaevskii, *Statistical Physics* (Pergamon, Oxford, 1980), Pt. II.
[31] Yu. S. Barash and V. L. Ginzburg, Usp. Fiz. Nauk **116**, 5 (1975); [Sov. Phys. Usp. **18**, 305 (1975)].
[32] F. Zhou and L. Spruch, Phys. Rev. A **52**, 297 (1995).
[33] G. L. Klimchitskaya, U. Mohideen, and V. M. Mostepanenko, Phys. Rev. A **61**, 062107 (2000).
[34] J. Blocki, J. Randrup, W. J. Swiatecki, and C. F. Tsang, Ann. Phys. (N.Y.) **105**, 427 (1977).
[35] T. Emig, R. L. Jaffe, M. Kardar, and A. Scardicchio, Phys. Rev. Lett. **96**, 080403 (2006).
[36] A. Bulgac, P. Magierski, and A. Wirzba, Phys. Rev. D **73**, 025007 (2006).
[37] M. Bordag, Phys. Rev. D **73**, 125018 (2006).
[38] H. Gies and K. Klingmüller, Phys. Rev. Lett. **96**, 220401 (2006); Phys. Rev. D **74**, 045002 (2006).
[39] E. Buks and M. L. Roukes, Nature (London) **419**, 119 (2002).
[40] D. Iannuzzi, M. Lisanti, and F. Capasso, Proc. Natl. Acad. Sci. U.S.A. **101**, 4019 (2004).
[41] F. Chen, G. L. Klimchitskaya, U. Mohideen, and V. M. Mostepanenko, Phys. Rev. Lett. **90**, 160404 (2003).
[42] F. Chen, U. Mohideen, and P. W. Milonni, in *Quantum Field Theory under the Influence of External Conditions*, edited by K. A. Milton (Rinton, Princeton, 2004).
[43] F. Chen, U. Mohideen, G. L. Klimchitskaya, and V. M. Mostepanenko, Phys. Rev. A **72**, 020101(R) (2005); **73**, 019905(E) (2006).
[44] F. Chen, U. Mohideen, G. L. Klimchitskaya, and V. M. Mostepanenko, Phys. Rev. A **74**, 022103 (2006).
[45] F. Chen, G. L. Klimchitskaya, V. M. Mostepanenko, and U. Mohideen, Phys. Rev. Lett. **97**, 170402 (2006).
[46] J. Opsal, M. W. Taylor, W. L. Smith, and A. Rosencwaig, J. Appl. Phys. **61**, 240 (1987).
[47] T. Vogel, G. Dobel, E. Holzhauer, H. Salzmann, and A. Theurer, Appl. Opt. **31**, 329 (1992).
[48] W. Arnold, S. Hunklinger, and K. Dransfeld, Phys. Rev. B **19**, 6049 (1979).
[49] F. Chen, G. L. Klimchitskaya, V. M. Mostepanenko, and U. Mohideen, Opt. Express **15**, 4823 (2007).
[50] B. Geyer, G. L. Klimchitskaya, and V. M. Mostepanenko, Int. J. Mod. Phys. A **21**, 5007 (2006).
[51] B. Geyer, G. L. Klimchitskaya, and V. M. Mostepanenko, Ann. Phys. (N.Y.), doi:10.1016/j.aop.2007.04.005.
[52] *Handbook of Optical Constants of Solids*, edited by E. D. Palik (Academic, New York, 1985).
[53] W. R. Smythe, *Electrostatics and Electrodynamics* (McGraw-Hill, New York, 1950).
[54] A. J. Sabbach and D. M. Riffe, Phys. Rev. B **66**, 165217 (2002).
[55] M. Nagai and M. Kuwata-Gonokami, J. Phys. Soc. Jpn. **71**, 2276 (2002).
[56] H. Angermann, Anal. Bioanal. Chem. **374**, 676 (2002).
[57] L. Kronik and Y. Shapira, Surf. Interface Anal. **31**, 954 (2001).
[58] S. G. Rabinovich, *Measurement Errors and Uncertainties: Theory and Practice* (Springer-Verlag, New York, 2000).
[59] G. L. Klimchitskaya, F. Chen, R. S. Decca, E. Fischbach, D. E. Krause, D. López, U. Mohideen, and V. M. Mostepanenko, J. Phys. A **39**, 6485 (2006).
[60] B. Geyer, G. L. Klimchitskaya, and V. M. Mostepanenko, Phys. Rev. A **72**, 022111 (2005).
[61] A. O. Caride, G. L. Klimchitskaya, V. M. Mostepanenko, Phys. Rev. A **71**, 042901 (2005).
[62] E. Yablonovitch, D. L. Allara, C. C. Chang, T. Gmitter, and T. B. Bright, Phys. Rev. Lett. **57**, 249 (1986).
[63] V. B. Bezerra, G. L. Klimchitskaya, and C. Romero, Mod. Phys. Lett. A **12**, 2623 (1997).
[64] M. Boström and B. E. Sernelius, Phys. Rev. Lett. **84**, 4757 (2000).
[65] I. Brevik, J. B. Aarseth, J. S. Høye, and K. A. Milton, Phys. Rev. E **71**, 056101 (2005).
[66] V. B. Bezerra, R. S. Decca, E. Fischbach, B. Geyer, G. L. Klimchitskaya, D. E. Krause, D. López, V. M. Mostepanenko, and C. Romero, Phys. Rev. E **73**, 028101 (2006).
[67] G. L. Klimchitskaya, U. Mohideen, and V. M. Mostepanenko, J. Phys. A **40**, 339(F) (2007).
[68] A. A. Maradudin and P. Mazur, Phys. Rev. B **22**, 1677 (1980).
[69] K. Joulain, J.-P. Mulet, F. Marquier, R. Carminati, and J.-J. Greffet, Surf. Sci. Rep. **57**, 59 (2005).
[70] G. L. Klimchitskaya, B. Geyer, and V. M. Mostepanenko, J. Phys. A **39**, 6495 (2006).
[71] J. M. Obrecht, R. J. Wild, M. Antezza, L. P. Pitaevskii, S. Stringari, and E. A. Cornell, Phys. Rev. Lett. **98**, 063201 (2007).